Fluid Dynamics & Materials Processing

Tech Science Press

DOI: 10.32604/fdmp.2023.025015

ARTICLE

A New Elastoplastic 3D Sand Production Model for Fractured Gas Fields

Hongtao Liu, Hongtao Jing, Zhixiong Tu*, Shiyong Qin, Junhui Wei and Xiaotong Yu

Tarim Oilfield Oil and Gas Engineering Research Institute, Korla, 841000, China

*Corresponding Author: Zhixiong Tu. Email: tuzx-txn@petrochina.com.cn

Received: 17 June 2022 Accepted: 11 October 2022

ABSTRACT

Reservoirs characterized by high temperature, high-pressure, medium high cementation strength, low porosity, and low permeability, in general, are not affected by sand production issues. Since 2009, however, it is known that cases exists where sand is present and may represent a significant technical problem (e.g., the the Dina II condensate gas field). In the present study, the main factors affecting sand production in this type of reservoir are considered (mechanical properties, stress fields, production system, completion method and gas flow pattern changes during the production process). On this basis, a new liquid-solid coupled porous elasto-plastic 3D sand production model is introduced and validated through comparison with effective sand production data. The related prediction errors are found to be within 15%, which represents the necessary prerequisite for the utilization of such a model for the elaboration of sand prevention measures.

KEYWORDS

Medium-high strength; sand production mechanism; fluid-solid coupling; sand production prediction; dynamic sand production pattern

1 Introduction

Sand production from oil and gas wells has always been one of the key technical problems restricting oil fields' efficient exploitation. Currently, a large number of researches are mainly focused on unconsolidated sandstone and weakly cemented sandstone reservoirs. Traditional views hold no sand production problem in medium-high-strength reservoirs [1]. The Dina II condensate gas field belongs to a sandstone gas reservoir in a fractured piedmont structural zone with high temperature, high pressure, and medium-high cementation strength. Since it was put into production in 2009, the number of sand production wells has increased yearly, and the sand production problem has become increasingly serious. Sand production leads to the blockage of downhole string, which seriously restricts the normal exploitation of this block. In order to reveal the sand production law of the Dina II gas field, it is necessary to clarify the sand production mechanism of this type of gas field.

Sand production from oil and gas reservoirs is a complex fluid-solid coupling process. The sand production process is manifested in two distinct phases, namely, the mechanical destabilization of rocks and the hydrodynamic transport process of particles [2,3]. To analyze the causes of sand production and sand production pattern in Dina II medium-high intensity reservoir then, it is necessary to clarify the sand production mechanism first. Research shows that sand production is mainly manifested in three

categories: mechanical mechanism (shear damage, tensile damage, and compression damage), fluid erosion mechanism, and pressure pulse mechanism.

On the one hand, the shear stress of stratum rock exceeds the shear strength of rock, which will cause sand production. On the other hand, the weak cementation caused by natural cracks and aweak surface will also cause sand production caused by weak shear strength, which is mainly manifested as a shear failure mechanism. Tensile failure usually occurs in weak sandstone formation, which is mainly caused by drag force generated by high-speed fluid. If the pore pressure gradient is larger than the radial stress gradient acting on the borehole wall or perforation, the effective radial stress will become tensile stress. When the effective radial stress is greater than the critical stress (i.e., the tensile strength of rock), tensile failure can be formed at a certain point on the well wall. Tensile failure occurs only in small holes like perforation holes, not in open holes. This is because in large cavities like open holes, shear failure always occurs before tensile failure [4,5]. Due to the size effect, the threshold of shear failure of small holes such as perforation holes is much higher, so the tensile failure may occur first. In the production process, tensile failure is sporadic, resulting in a small sand production, which is generally stable with time. To prevent sand production in the early stage of oil and gas well production, the critical rate of wellbore pressure drop should be considered. In the experiment of radial flow hollow cylinder sample, the failure mode of pore collapse volume failure was found. This kind of volume failure is closely related to the production pressure difference and the degree of oil and gas reservoir depletion. Generally, it occurs in high pressure, high porosity and low strength oil and gas reservoirs [6,7]. Due to the increase of average stress caused by long-term production, when the average stress exceeds the upper limit pressure of volume damage, sand production will be caused. This failure feature can make the formation form a fracture failure area, which starts from the top of the initial shear failure area. When the fluid flows, the broken rock particles will erode, which will move with the fluid. With the strengthening of erosion force, cracks will be formed on the rock surface of the formation, resulting in a large amount of sand production [8,9].

In addition to mechanical failure causing sand out, fluid erosion of the pore surfaces inside the stratigraphic rocks will produce some fine rock particles and transport them with the fluid, exhibiting rock erosion damage. The erosion inside the rock may be related to the micromechanical impact acting on the rock skeleton, causing viscous shear of the solid particles transported in the pore network, and the surface erosion of the rock is the result of the combined effect of free-surface parallel flow and vertical flow with the surface. Since the dynamics of fluid flow is the main cause of sand grain transport, fluid erosion, as well as the amount of sand coming out of the formation is related to fluid velocity, fluid viscosity, fluid density, sand grain shape, and sand grain size [10–12].

In recent years, it has been observed that the quick opening and closing of oil and gas wells in the field often leads to sudden sand production, changing the working system. Sudden momentum change may produce a pressure cycle pulse, which will cause damage to reservoir rocks. In the light, it will cause erosion and damage of sand particles, and in the heavy, it will accelerate the decline of rock strength, thus accelerating the production of sand particles. This type is the mechanism of the pressure pulse.

The calculation speed of the sand production model is very fast, but there are some limitations. Usually, they can only predict the beginning of sand production, but not the amount of sand production, which is also very important for the design of a sand production management system. Most of these models only consider one failure mechanism, which is not enough in most cases, so they cannot be applied to all fields [13,14]. These models are limited to simple geometry and boundary conditions, which may not be suitable for real field conditions (such as perforated wells, deviated wells and fractured wells). Finally, these models do not consider plasticity, essential in any sand layer damage and production model. In order to accurately predict the beginning and amount of sand production, different mechanical failure mechanisms, plasticity, cavities with complex shapes, and fluid erosion must be considered in the sand production model.

Sand production mechanism in Dina II gas field mainly shows the interaction of mechanics, fluid erosion, and pressure excitation. On the basis of a comprehensive analysis of the sand production mechanism of the Dina II condensate gas field, this paper comprehensively considers the factors such as mechanical characteristics, *in-situ* stress field, production system, completion methods, and gas flow pattern changes during exploitation. It develops a new set of porous elastic-plastic 3D sand production fluid-solid coupling models to predict the sand production in the whole area of Dina II gas field, thus revealing the vertical and horizontal dynamic sand production pattern in the whole well area of this gas field.

2 Fluid-Solid Coupling Model of Porous Elastoplastic 3D Sand Production

The accurate prediction of sand production has been the focus of research by scholars at home and abroad, which involves theories from multiple disciplines such as porous elastic media mechanics, rock mechanics, fluid mechanics, and oilfield chemistry, and is influenced and controlled by a variety of factors such as formation mechanics, fluid properties, well completion and production processes. The development of sand prediction methods has gone through a tortuous development process from simple to complex and from qualitative to quantitative. It mainly includes the following stages: field engineering method, mechanistic analytical model, and fluid-solid coupling model.

The field engineering method is used to establish empirical relationships between oil and gas well sand production data and field parameters, such as establishing relationships between sand production and sonic time difference, production rate, production pressure difference, oil recovery index, water content, and gas content. Although the empirical formula can also predict sand production well, it requires a large amount of production practice information; it does not apply to blocks that have just been put into production, and its scope of application is greatly limited. The analytical equation for the amount of sand is obtained by using the material balance method, which does not consider whether the fluid has sufficient flow velocity to carry the sand particles to the surface, and the prediction result is often high.

A reservoir is a porous medium in which the solid, liquid, and gas phases coexist. In the process of oil and gas production, the production of oil and gas leads to the change of reservoir pore pressure and redistribution of stress, thus deforming the rock skeleton and changing both porosity and permeability, affecting the flow of fluid in the pore space. Therefore, the oil and gas production process are a fluid-solid coupling process, and the sand production in the oil and gas production process is also a fluid-solid coupling process. In this paper, a new three-dimensional multiphase porous elastoplastic numerical model was elaborated based on the research of Wang et al. [15–17], which can be used to quantitatively evaluate the sand production failure, critical sand production state, and sand production volume under different conditions. The model employs an improved Moore-Coulomb criterion to capture shear, tensile, and compression damage phenomena. And the post-yielding behavior of rocks, such as rock plasticity or strain hardening/softening, can be simulated. The model also satisfies both mechanical damage and fluid erosion criterion, i.e., when the drag force is greater than the resistance, it causes sand outflow.

2.1 Multiphase Flow and Coupling with Rock Deformation

Assuming that the multiphase fluids (water, gas, and oil) are immiscible and micro-compressible, to derive the pore elasticity equations, we combine Biot's theory of pore elasticity and a modified Moore-Coulomb cap model to calculate the incremental plastic strain. The two control equations are iteratively coupled to obtain the pressure (p) and incremental displacement (du).

$$\frac{\partial p}{\partial t} = \frac{kM}{\mu_f}\nabla^2 p - \alpha M \frac{\partial(\nabla \cdot u)}{\partial t} \tag{1}$$

$$\frac{\partial^2(\rho u)}{\partial t^2} = \nabla \cdot \left[G\nabla du + G(\nabla du)^T + \lambda Itr(\nabla du)\right] - \nabla \cdot \left[2G\left(d\varepsilon_p\right) + \lambda Itr\left(d\varepsilon_p\right)\right] + \nabla \cdot \left(\sigma^{old} - \alpha pI\right) \tag{2}$$

κ-Permeability; M-Biot modulus; u_f-Fluid viscosity; α-Biot coefficient; G-Shear modulus; ε_p-Plastic strain tensor; σ^{old}-*In-situ* stress tensor.

2.2 Establish the Dynamic Multiphase Component Equation

For multiphase components, the component equilibrium equation is obtained by combining the multiphase non-Darcy's law and the mass conservation equation.

$$\frac{1}{V}\frac{\partial N_i}{\partial t} - \nabla \cdot \sum_{j=1}^{N_p} \xi_j x_{ij} k \frac{k_{rj}}{\mu_j} \nabla\left(p + p_{cj}\right) - \nabla \cdot \sum_{j=1}^{N_p} \xi_j x_{ij} k \frac{k_{rj}}{\mu_j} \beta_j \rho_j |v_j| \cdot v_j = 0 \tag{3}$$

where i represents the number of moles per unit time of each component and j represents the water, oil or gas phase.

2.3 Establish the Pressure Equation

The pressure equation is obtained using the constraint that the pore volume of the deformed pore medium must be filled with fluid.

$$\frac{1}{M}\frac{\partial p}{\partial t} - \sum_{i=1}^{N_c+1} \frac{\partial V_t}{\partial N_i} \nabla \cdot \sum_{j=1}^{N_p} \xi_j x_{ij} k \frac{k_{rj}}{\mu_j} \nabla\left(p + p_{cj}\right) - \sum_{i=1}^{N_c+1} \frac{\partial V_t}{\partial N_i} \nabla \cdot \sum_{j=1}^{N_p} \xi_j x_{ij} k \frac{k_{rj}}{\mu_j} \beta_j \rho_j |v_j| \cdot v_j + \alpha \frac{\partial(\nabla \cdot u)}{\partial t} = 0 \tag{4}$$

N_c-Number of components; V_t-Fluid volume.

2.4 Calculate the Cumulative Plastic Strain

Based on a three-dimensional pore elastic-plastic model, the pore pressure transients and rock deformation are calculated using a coupled approach. Combined with the improved Moore-Coulomb cap criterion, the cumulative plastic strain can be obtained by using different yield conditions to limit the stress. The shear yield surface, tensile yield surface, and compression yield surface are expressed as

$$f^s = \sigma_1 - \frac{1 + sin\varphi}{1 - sin\varphi}\sigma_3 + 2c\sqrt{\frac{1 + sin\varphi}{1 - sin\varphi}} \tag{5}$$

$$Af^t = \sigma_3 - \sigma_t = \sigma_3 - t_{cutoff}\frac{c}{tan\varphi} \tag{6}$$

$$f^c = \frac{1}{3}(\sigma_1 + \sigma_2 + \sigma_3) + p^{cap} \tag{7}$$

where φ is Friction Angle.

In most cases, shear and tensile yield surfaces are sufficient to calibrate rock damage behavior, however, if the rock exhibits strong compaction at high stresses and fails due to pore collapse, neither shear nor tensile yield criteria are valid. For this situation, a compression yield surface is proposed to determine the occurrence of compression yield damage under high-stress conditions when the average stress exceeds a critical value.

2.5 Sand Erosion Damage

Rocks can withstand a certain amount of plastic strain before they are destroyed, the magnitude of which depends on the rock properties (lower critical plastic strain if the rock is weak, higher critical plastic strain if

the rock is ductile). However, rock failure does not imply sand production; it is assumed that the failed rock forms sand grains that remain in the formation until the drag force acting on the grains exceeds the resistance that holds the grains in place, and then the production behavior occurs. For this reason, the shape drag and friction drag calculation equations are introduced into the model and calculated as follows:

$$F_{drag,j} = \pi r^2 \left(\frac{1}{2}\rho_j v_j^2\right) f \tag{8}$$

where f is the friction coefficient.

3 Sand Production Mechanism and Prediction Model

A porous elastoplastic 3D sand production fluid-solid coupling model can be used to calculate pore pressure transient and rock deformation. Rock can bear a certain plastic strain before it is destroyed. The magnitude of this strain depends on the nature of the rock, which can be obtained from triaxial tests and other experiments. If the thresholds of rock failure and fluid erosion are met simultaneously, sand production will occur. To effectively capture the strain concentration area before and after cavity expansion after sand production, a dynamic mesh refinement/non-refinement algorithm is implemented in the model.

3.1 Failure Mechanism of Rock Deformation

Tensile failure: When the minimum principal stress exceeds the tensile strength, tensile yield occurs. For problems related to sand production can be triggered by mechanical or fluid flow effects. Mechanically speaking, if the stress contrast is very large, tensile stress may appear along the direction of maximum stress around the well, resulting in tensile yield. On the other hand, if the pressure drop is large, the radial stress caused by pressure may exceed the tensile strength of the rock. In this models, the tensile plastic strain will be calculated once the tensile yield occurs. If the accumulated tensile plastic strain is greater than the critical value, the tensile failure is achieved, and the damaged sand is ready for fluid erosion.

Shear failure: Shear yield occurs when shear stress exceeds shear strength. In the Mohr-Coulomb model, shear strength is controlled by cohesion and internal friction angle, while shear stress is related to maximum and minimum principal stress. Like tensile yield, shear yield is also affected by mechanical and fluid flow effects. Contrary to mechanical instability, shear yield is affected not only by stress contrast but also by stress magnitude. The greater the stress contrast and stress, the more likely it is that sand will yield in shear mode. From the point of view of fluid flow, both injection and production will lead to shear yield. In the injection process, the effective stress decreases with the increase of pore pressure, and the Mohr circle moves to the yield surface. In the production process, the decrease of pore pressure will increase the effective stress, but due to the porous elastic effect, the amount of increase is different. This may cause Mohr's circle to move towards the yield surface. Once the shear yield occurs, the shear plastic strain is calculated. Once the accumulated shear plastic strain exceeds the critical value (obtained from the experiment), the shear failure in the model is detected.

Volume failure: In high porosity reservoirs with low compaction strength, volume failure (compression failure) may occur during production. With the exploitation of oil/natural gas, the depletion of the reservoir leads to an increase of average effective stress (near wellbore/perforation/fracture). Once the compaction strength is exceeded, the volume yield begins, and the volume plastic strain is obtained. Volume failure occurs when the cumulative volume plastic strain is greater than the critical volume plastic strain.

3.2 Fluid Erosion Mechanism

As long as one type of damage is achieved, the damaged rock is considered to be degraded into sand grains. They will remain in the formation until the resistance acting on the sand exceeds the resistance to

keep the sand in place. In this model, the dynamic force of any phase (oil, water, or gas) on the failed sand layer consists of formal resistance and frictional resistance. It is calculated as the general form by Eq. (9)

$$F_{drag,j} = \pi r^2 \left(\frac{1}{2}\rho_j v_j^2\right) f \tag{9}$$

The friction coefficient (f) in this formula is a nonlinear function of the Reynolds number, which is mathematically defined as (10)

$$f = \begin{cases} \dfrac{24}{Re}, \; for \; Re < 0.1 \\ \left(\sqrt{\dfrac{24}{Re}} + 0.5407\right)^2, \; for \; 0.1 < Re \leq 500 \\ 0.44, for \; Re \geq 500 \end{cases} \tag{10}$$

Reynolds number of any fluid phase is expressed as

$$Re_j = \frac{2R_{sand} v_j \rho_j}{\mu_j} \tag{11}$$

From the above definition, we can observe a non-unique relationship between resistance and fluid velocity: for peristaltic flow, resistance is linearly proportional to velocity; However, with the increase of Reynolds number, there is a nonlinear proportional relationship between resistance and velocity. Finally, in turbulent flow, the resistance on sand is proportional to the square of fluid velocity.

On the other hand, the resistance consists of gravity and capillary cohesion (multiphase only) acting on the sand. Because the capillary cohesion is much smaller than the rock cohesion, it is not included in the failure calculation. However, capillary cohesion is very important in fluid erosion, because it increases considerable resistance to prevent the failed sand from being eroded. Therefore, the resistance of sand particles in any fluid phase is calculated by the formula for multiphase fluid flow, as shown in Eq. (12). C_{cap} is capillary cohesion depending on capillary pressure.

$$F_{resistance,j} = \frac{4}{3}\pi r^3 \left(\rho_{sand} - \rho_j\right) g + 4\pi r^2 C_{cap} \tag{12}$$

In addition, the capillary pressure of the water-oil system with water as the wetting phase is calculated using the correlation shown below:

$$p_c = p_c^0 \left(1 - \frac{S_w - S_{wr}}{1 - S_{wr} - S_{or}}\right)^{Epc} \tag{13}$$

The capillary cohesion depends on capillary pressure, water saturation, and internal friction angle, and is calculated by using the Eq. (14).

$$C_{cap} = S_w \cdot p_c \cdot tan\varphi \tag{14}$$

3.3 Sand Production Calculation

Sand production will occur only when the criteria of rock failure and fluid erosion are met simultaneously. Once these two criteria are met in this model, a new dynamic cell removal algorithm is implemented to represent sand entrainment.

According to the previous experiment and field observation, the oil well/perforation produces sand. Therefore, a cell removal method based on surface corrosion was developed. We check the units on the production surface for faults and fluid erosion. If these two criteria are met, they will be deleted from the

grid system. This leads to the topological change of the well/perforation interface, which requires the current stress/pore pressure boundary conditions to be applied to the newly exposed surface (now a part of the well/perforation interface). As the geometry has been changed, the stress and pore pressure distributions are recalculated to achieve balance before the next simulation step.

Sand production is calculated according to the removed pore volume and porosity.

$$V_{sand} = (1 - \varphi) \sum V_{removed\ element} \tag{15}$$

4 Sand Production Pattern in Dina II Gas Field

A three-dimensional multi-phase porous elastoplastic sand production prediction numerical model is elaborated to predict sand production from the Dina II gas field, analyze the sand production mechanism, and reveal the sand production pattern in the whole well area. The model requires obtaining five aspects of information, such as reservoir strength, reservoir physical properties, stress distribution, completion method and production curve, etc. Based on this, the whole calculation process is elaborated.

4.1 Single Well Sand Production Analysis

In this paper, more comprehensive rock mechanics experimental data, drilling and completion data, logging data, recording data, and daily production data of 18 wells in the Dina II gas field were collected to carry out the quantitative calculation of the sand production in the whole well area. When taking X-22 well as an example, the time of sand production and the prediction of sand production volume was carried out.

(1) Overview

Well X-22 is a development well on Dina II gas field. The well was drilled on February 14th, 2009, and drilled to a depth of 5242.0 m on June 6th, 2009. According to the geological design, the well was drilled in the mudstone above the top boundary of the third member of the Kumgelemu Group. The well is completed by casing perforation. The production zones are Paleogene Suweiyi Formation ($E_{2\text{-}3}s$) and Kumgelemu Formation ($E_{1\text{-}2}km_2$). The perforated interval of X-22 is 4894.50~5209.00 m by using 127 mm perforating gun group, and perforation parameters is 16 holes/m density, 7.6 mm hole diameter, and 60° perforation phase.

(2) Production curve

The well was put into production on September 17, 2009, with an oil pressure of 85 MPa. In October 2009, the choke was adjusted, and the oil pressure dropped to 80 MPa. Since 2012, sand production has been found at the wellhead of this well every year. On April 13th, 2015, the metering pipeline was shut down due to sand production in this well. To control the abnormal casing pressure, the operator decided to bean up the choke however, the sand production became more serious, and the choke needed to be cleaned almost every day.

(3) Analysis of critical sand production state: This well's formation pressure gradually decreases from 100 to 74 MPa in the production process, and the degree of pressure depletion is over 30%. Therefore, it is necessary to consider the influence of pressure depletion on the critical sand production pressure and analyze the critical sand production state under different reservoir pressures; calculation parameters are shown in Table 1.

The calculation shows that when the reservoir pressure is at 100 MPa and the bottom hole pressure is greater than 80 MPa which means the pressure drawdown is less than 20 MPa and the whole reservoir is in the green sand-free zone without failure damage. However, as the reservoir pressure decreases and the bottom hole pressure is less than 80 MPa, the rock failure damage starts to occur as well as sand production, and the critical sand production pressure drawdown is greater than 20 MPa, as shown in Fig. 1.

Table 1: Calculation parameters

Gas group	Well completion method	Well depth/m	Pp/MPa	Biot coefficient/1	Porosity /%	Permeability/mD	Young's modulus/MPa
$E_{1\text{-}2}km_2$	Cased hole completion	5157–5209	102.41	1	0.09	0.9	46492
Poisson's ratio/1	**Cohesion/** MPa	**Friction angle/°**	**Compressive strength (UCS)/**MPa	**Overlying stress/**MPa	**Maximum horizontal stress/**MPa	**Minimum horizontal stress/**MPa	
0.22	22.9	25.2	91.63	129.17	134.39	119.6	

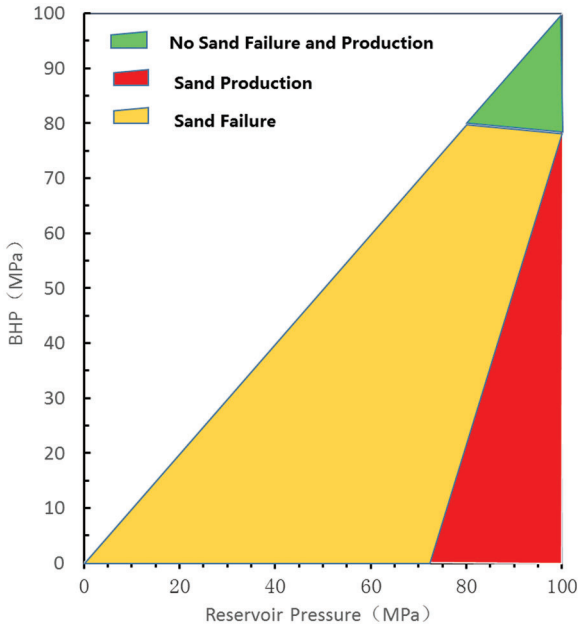

Figure 1: Tri-color diagram of X-22 well critical sand production state

(4) Effect of rock strength on sand production

Through the model prediction, different sand production levels can be found from different layers of the reservoir because these layers have different rock strengths. When the layer strength is greater than 27.52 MPa ($E_{2\text{-}3}s_1$) less volume of sand production is predicted. However, when the rock cohesion is reduced to 22.9 MPa ($E_{2\text{-}3}s_2$) we can see the sand production volume increases sharply. The key sand emission in this well is in the $E_{1\text{-}2}km_2$ layer, as shown in Fig. 2.

(5) Analysis of sand production throughout the production cycle

By calculating the sand production volume for the whole production cycle of the X-22 well, it can be seen that sand production starts to occur from 2012 when the pressure drawdown is greater than 20 MPa, the critical pressure drawdown will further decrease as the reservoir pressure is depleted, as shown in Fig. 3. Fig. 3 also shows that sand production increased sharply during 2015.

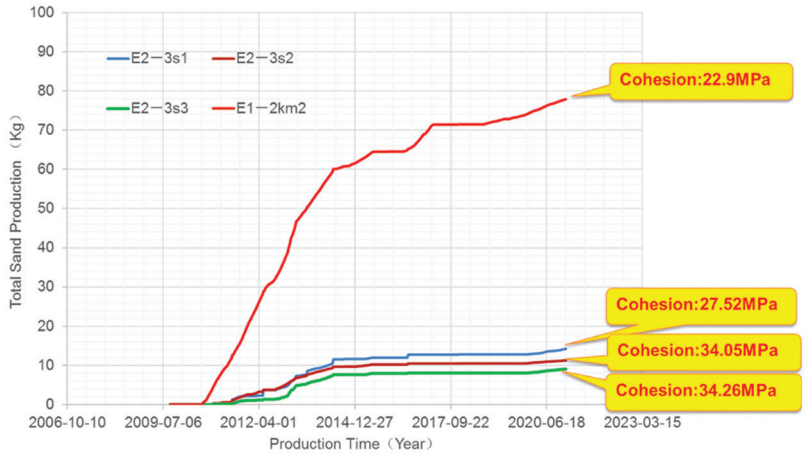

Figure 2: Cumulative sand production curve of different reservoirs in X-22 well

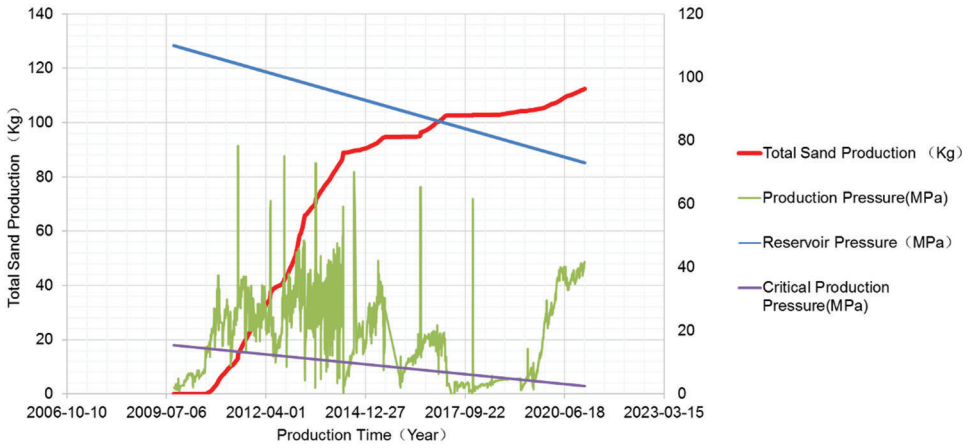

Figure 3: Cumulative sand production curve of X-22 well

During the production period, sand was found at the wellhead of the well every year since 2012, and the well was shut down on April 13, 2015, due to sand plugging the metering line as a result of more serious sand production in the well. To control the abnormal casing pressure of the well then, the choke had to be beaned up, so the sand situation became more serious, and the choke had to be disassembled and cleaned almost every day. The prediction is also consistent with the sand production observation onsite.

4.2 Analysis of Sand Production Pattern in Dina II Gas Field

By calculating the sand production volume of all production wells in the Dina I gas field, the distribution pattern of different well locations and production periods is investigated and obtained. The analysis reveals that the sand production wells in the whole area have a certain pattern from 2009 to the present and can be divided into four time periods according to the severity of sand production, as shown in Fig. 4.

(1) Stage 1: 2009–2010, belongs to the stage of no sand production. There is no sand production in the whole region at this stage.

(2) Stage 2: 2011–2014, belongs to the stage of small amount of sand production. The amount of sand production increases linearly and slowly with time, and the sand production region is close to wells X-6/7/8 and X-23.

(3) Stage 3: 2015–2018, sand production increases sharply, and the sand production rate increase faster with time which means the growth slope becomes steeper, and the sand production region gradually expands from X-6/7/8 wells and near X-23 wells to X-5 wells and X-B1 wells.

(4) Stage 4: 2019 to present, belongs to the stage of sand production; the sand production volume in this phase no longer increases significantly and tends to be stable. The sand production region furtherly expands to X-1/2/4/10/11/12/22 wells and X-B/2 wells.

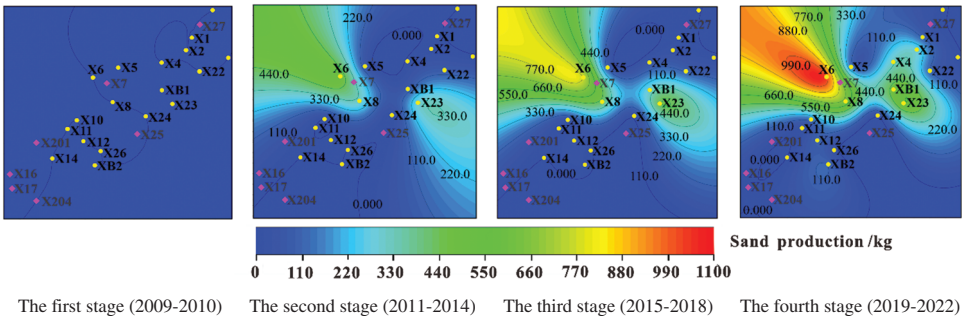

Figure 4: Sand production pattern at different production stages of Dina II gas field

4.3 Model Validation

On-site sand monitoring was conducted on eight wells using the CLAMP-ON ultrasonic sand production monitor equipment from June 2018 to August 2018, and the field test data were compared and analyzed with model calculations to obtain the error range of sand production prediction. As shown in Fig. 5 the average prediction accuracy is 87.54%, as shown in Fig. 5. The higher error in individual wells may be because the failure formation sand was not carried to the surface; therefore the sand monitor was notable to catch this part of sand production at formation.

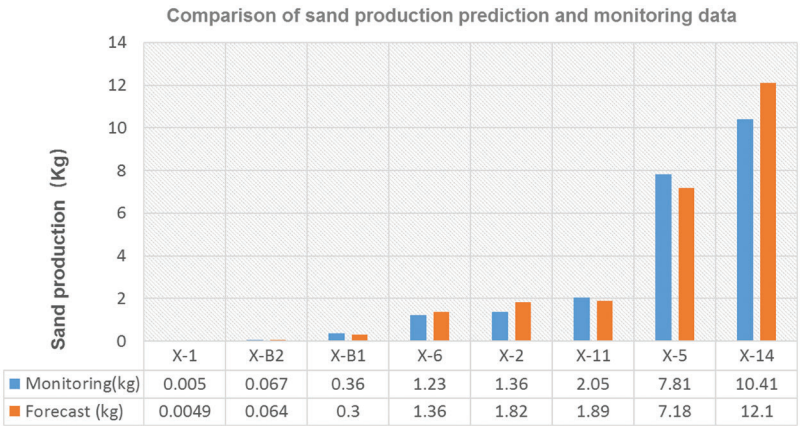

Figure 5: Comparison of monitoring and prediction data from Dina II gas field (June 2018 to August 2018)

5 Conclusion

The Dina II gas field is a high-pressure, low porosity, low permeability, medium-high-strength fractured sandstone reservoir with a low risk of initial sand production, and gradually starts to produce sand as the reservoir pressure depleted along with the production process, which indicates that the there is a multifactorial coupling mechanism causes sand production of this gas field combining mechanical damage, fluid erosion damage, and pressure pulse which also causes the difficulty in sand production prediction.

The analysis of the sand production pattern in this gas field shows that sand production has an obvious time effect, and the whole area can be divided into four time periods according to the severity of sand production: no sand production stage, small amount of sand production stage, intensive sand production stage and stable sand production stage. From the well location aspect, the area of heavy sand production is around X-6/7/8 wells, and the area of medium sand production is around X-B1 and X-23 wells.

The new poroelastic-plastic 3D sand fluid-solid coupling model in this paper is the first model to calculate transient and steady-state flow and deformation, combining multiphase flow and capillary forces, and capturing complex post-yield behavior such as strain hardening/softening, etc. Field sand monitoring data verify the model, and the prediction error can be controlled within 15%, which can provide basic theoretical support for oilfields to formulate reasonable sand prevention measures and effective development methods.

The new sand production model elaborated in this paper realizes the accurate prediction and evaluation of sand production. It could replace the expensive sand production monitoring instrument, greatly saves the field completion cost, and has a high field application value. The shortcoming of this method is that it does not consider the influence of specific sand control measures on sand production, and further research should be carried out based on the influence pattern of sand control on sand production.

Funding Statement: This study has been supported by the Major Science and Technology Project "Comprehensive Research of Exploration Matching and Application of New Technology" (2016ZX5051-3) of CNPC.

Conflicts of Interest: The authors declare that they have no conflicts of interest to report regarding the present study.

References

1. Shaima, S., Adel, A., Yahya, W. (2013). Three dimensional modeling for predicting sand production. *Journal of Petroleum Science and Engineering, 109(2),* 348–363. https://doi.org/10.1016/j.petrol.2013.04.015
2. Perera, M. A., Ranjith, P. G., Rathnaweera, T. D., de Silva, G. P. D., Liu, T. (2017). An experimental study to quantify sand production during oil recovery from unconsolidated quicksand formations. *Petroleum Exploration and Development, 44(5),* 860–865. https://doi.org/10.1016/S1876-3804(17)30097-6
3. Khamitov, F., Minh Nguyen, H., Zhao, Y. (2022). Numerical investigation of sand production mechanisms in weak sandstone formations with various reservoir fluids. *International Journal of Rock Mechanics and Mining Sciences, 154(1–2),* 105096. https://doi.org/10.1016/j.ijrmms.2022.105096
4. Shabdirova, A., Nguyen, H. M., Zhao, Y. (2019). A sand production prediction model for weak sandstone reservoir in Kazakhstan. *Journal of Rock Mechanics and Geotechnical Engineering, 11(4),* 760–769. https://doi.org/10.1016/j.jrmge.2018.12.015
5. Jin, Y. R., Li, Y. L., Wu, N. Y., Yang, D. Y. (2022). Characterization of sand production for clayey-silt sediments conditioned to openhole gravel-packing: Experimental observations. *SPE Journal, 26(6),* 1–18. https://doi.org/10.2118/206708-PA

6. Soroush, M., Roostaei, M., Seyed, A. H., Mohammad, M., Peyman, P. et al. (2021). Challenges and potentials for sand and flow control and management in the sandstone oil fields of Kazakhstan: A literature review. *SPE Drilling & Completion, 36(1),* 208–231. https://doi.org/10.2118/199247-PA
7. Song, Y. Q., Ranjith, P. G., Wu, B. L., Song, Z. L. (2021). A microscopic study of sand arches and sand skeletons under hydrodynamic force based on the CFD-DEM model. *Journal of Natural Gas Science and Engineering, 92,* 104017. https://doi.org/10.1016/j.jngse.2021.104017
8. Dong, C. Y., Zhou, B., Huang, F. S., Zhang, L., Zhao, Y. Z. et al. (2022). Microscopic sand production simulation and visual sanding pattern description in weakly consolidated sandstone reservoirs. *Petroleum Science, 19(1),* 279–295. https://doi.org/10.1016/j.petsci.2021.09.039
9. Xia, T., Feng, Q. H., Wang, S., Zhang, J. Y., Zhang, W. et al. (2022). Numerical study and force chain network analysis of sand production process using coupled LBM-DEM. *Energies, 15(5),* 1–20. https://doi.org/10.3390/en15051788
10. Yu, H. S., Leung, J. (2020). A sand-arch stability constrained dynamic fractal wormhole growth model for simulating cold heavy-oil production with sand. *SPE Journal, 25(6),* 3440–3456. https://doi.org/10.2118/193893-PA
11. Aliyu, A. S., Lim, L. T. (2020). Modified approach for identifying weak zones for effective sand management. *Journal of Petroleum Exploration and Production Technology, 10(2),* 537–555. https://doi.org/10.1007/s13202-019-00784-5
12. Asad, A., Awotunde, A., Jamal, M. (2021). Simulation of wellbore erosion and sand transport in long horizontal wells producing gas at high velocities. *Journal of Natural Gas Science and Engineering, 89(33),* 103890. https://doi.org/10.1016/j.jngse.2021.103890
13. Ebikapaye, P., Gbenga, O., Nadimul, H. F. (2022). Sand production due to chemical-rock interaction. A review. *Engineering Failure Analysis, 142(2),* 106745. https://doi.org/10.1016/j.engfailanal.2022.106745
14. Ranjith, P. G., Perera M. S. A., Perera W. K. G., Choi, S. K., Yasar, E. (2014). Sand production during the extrusion of hydrocarbons from geological formations: A review. *Journal of Petroleum Science and Engineering, 124(2),* 72–82. https://doi.org/10.1016/j.petrol.2014.10.017
15. Wang, H. T., Sharma, M. (2019). The role of elasto-plasticity in cavity shape and sand production in oil and gas wells. *SPE Journal, 24(2),* 744–756. https://doi.org/10.2118/187225-PA
16. Wang, H. T., Hwang, J., Mukul, S. (2019). Sand production caused by water hammer events: Implications for shut-in protocols and design of water injection wells. *SPE Production & Operations, 34(3),* 461–472. https://doi.org/10.2118/189568-PA
17. Liu, H. T., Wang, H. T., Zhang, W., Liu, J. Y., Zhang, Y. T. et al. (2021). Predicting sand production rate in high-pressure, high-temperature wells in the Tarim Basin. *SPE Production & Operations, 36(1),* 174–196. https://doi.org/10.2118/191406-PA